

Keywords: pancreatic cancer; adenocarcinoma; PanIN; HMGA1; high-mobility group A protein

HMGA1 expression levels are elevated in pancreatic intraepithelial neoplasia cells in the Ptf1a-Cre; LSL-KrasG12D transgenic mouse model of pancreatic cancer

Michelle J Veite-Schmahl¹, William C Joesten¹ and Michael A Kennedy^{*,1}

¹Department of Chemistry and Biochemistry, Miami University, 651 E. High St., Oxford, OH 45056, USA

Background: Pancreatic cancer is currently the third leading cause of cancer deaths in the United States and it is predicted to become the second by the year 2030. High-mobility group A1 protein (HMGA1) is an oncogenic transcription factor, localised and active in cell nuclei, that is linked to tumour progression in many human cancers, including pancreatic cancer. Overexpression of HMGA1 renders cancer cells resistant to chemotherapy. Although the Ptf1a-Cre; LSL-KrasG12D transgenic mouse is perhaps the most widely utilised animal model for human pancreatic cancer, expression levels of HMGA1 in pancreata from this mouse model have not been characterised.

Methods: Quantitative immunohistochemical analysis was used to determine nuclear HMGA1 levels in pancreatic tissue sections from Ptf1a-Cre; LSL-KrasG12D mice aged 5, 11, and 15 months. The H Score method was used for quantitative analysis.

Results: The HMGA1 levels were significantly elevated in pancreatic intraepithelial neoplasia (PanIN) epithelia compared with untransformed acinar tissues or fibroinflammatory stroma.

Conclusions: The PanINs have long been regarded as precancerous precursors to pancreatic adenocarcinoma. Significantly elevated HMGA1 levels observed in the nuclei of PanINs in Ptf1a-Cre; LSL-KrasG12D mice validate this animal model for investigating the role that HMGA1 plays in cancer progression and testing therapeutic approaches targeting HMGA1 in human cancers.

Pancreatic cancer (PC) is currently estimated to be the third leading cause of cancer related deaths in the United States (<https://cancerstatisticscenter.cancer.org/#/>) with a 5-year survival of <10% (Warshaw and del Castillo, 1992; Hingorani *et al*, 2003; Jemal *et al*, 2006; Ottenhof *et al*, 2009; Rahib *et al*, 2014; Siegel *et al*, 2016; American Cancer Society, 2017). Exocrine tumours in the pancreas account for over 95% of all pancreatic malignancies (Fesinmeyer *et al*, 2005). Specifically, pancreatic ductal adenocarcinoma (PDAC) comprises ~90% of these exocrine tumours and resists all conventional forms of chemotherapy and radiotherapy (Futura *et al*, 1992; Yadav and Lowenfels, 2013). Surgery is

currently the most effective treatment for patients with PC. Unfortunately, most patients are not candidates for resection because of metastases or extensive local vascular involvement at diagnosis (National Cancer Institute, 2014; <https://deainfo.nci.nih.gov/advisory/ctac/workgroup/pc/PDACframework.pdf>). Despite surgery being the most effective method of treatment, only 3–4% of all patients who undergo resection receive a disease-free diagnosis with long-term survival. Precancerous lesions, referred to as pancreatic intraepithelial neoplasms (PanINs), are below the detection limit of current imaging capabilities (Chari *et al*, 2015). In 2014, there were 39 590 deaths as a result of PC (Stark and Eibl,

*Correspondence: Professor MA Kennedy; E-mail: Kennedm4@miamioh.edu

Received 4 April 2017; revised 2 June 2017; accepted 14 June 2017; published online 11 July 2017

© 2017 Cancer Research UK. All rights reserved 0007–0920/17

2015) and in 2017 it is estimated that there will be 43 090 deaths because of PC (<https://cancerstatisticscenter.cancer.org/#/>). Because of the substantial amount of deaths and low survival rates, many researchers have directed their attention towards discovering methods of earlier detection of PC and development of new therapeutic approaches to treat PC.

High-mobility group A1 protein (HMGA1) is implicated in many human cancers, including PC. It is a non-histone chromatin architectural transcription factor that changes the structure of chromatin upon binding and can cause unwinding of DNA during transcription. The change to chromatin structure allows increased access to euchromatin that can result in both altered upregulation and downregulation of effected genes. The HMGA1 is expressed at high levels during embryogenesis, but is generally expressed at relatively low levels in adult tissues, thus suggesting a critical role in development (Fusco and Fedele, 2007). It is often expressed at higher than normal levels in cancer cells, and because its overexpression naturally leads to misregulation of affected genes, this contributes to tumour initiation and progression. Elevated HMGA1 expression levels in cancer cells have been associated with tumour progression, metastatic ability, and a reduced survival rate (Fusco and Fedele, 2007; Kolb *et al*, 2007; Hristov *et al*, 2010) and higher levels of HMGA1 are generally associated with more advanced tumours (Fusco and Fedele, 2007). Elevated HMGA1 expression levels have also been correlated with increased cancer cell resistance to chemotherapy (Liau and Whang, 2008) by mechanisms that are not fully understood; however, suppression of HMGA1 expression (Puca *et al*, 2014) or sequestration of elevated HMGA1 levels by competitive binding to DNA aptamer decoys (Watanabe *et al*, 2012) have been shown to increase cancer cell sensitivity to chemotherapy. The association of HMGA1 with tumour cell progression, increased metastatic potential, and chemotherapy resistance in cancer cells has led to HMGA1 now being considered a prognostic biomarker for many cancers and there is increased interest in HMGA1 as a therapeutic target for treating cancer (Liau and Whang, 2009; Shah and Resar, 2012).

Mouse models are widely used as models to study human cancers, and to study the efficacy of new therapeutic strategies. The Ptf1a-Cre; LSL-KrasG12D mouse model is one of the most widely used and best characterised models of PC. In this model, one strain of mouse containing an oncogenic G12D Kras mutant that is silenced under a Lox-Stop-Lox cassette, that is, the LSL-KrasG12D strain originally developed by the Tyler Jacks group at the Massachusetts Institute of Technology (Jackson *et al*, 2001; Johnson *et al*, 2001; Tuveson *et al*, 2004), is cross-bred with a second strain of mouse that contains a Cre-recombinase capable of unsilencing the oncogenic Kras oncogene, but whose expression is restricted to the pancreas by placing the Cre-recombinase expression under the control of a promoter expressed specifically in the pancreas, in this case Ptf1a, originally developed by Chris Wright group (Kawaguchi *et al*, 2002), that is named Ptf1a-Cre (Hingorani *et al*, 2003; Tuveson *et al*, 2004). Cross-breeding the two strains statistically produces 25% of the offspring that carry both genetic alterations and that are capable of expression of the KrasG12D mutant selectively in the pancreas (Hingorani *et al*, 2003). Expression of the mutant Kras specifically in the pancreas results in extensive PanIN formation throughout the pancreas, and the PanINs have been shown to progress to PDAC (Hingorani *et al*, 2003). By utilising this transgenic mouse model, it is possible to investigate PC progression starting from the earliest precancerous PanIN stages through cancer initiation, tumour progression, and metastasis.

Here, we have used the Ptf1a-Cre; LSL-KrasG12D model, in combination with quantitative immunohistochemistry (IHC), to investigate HMGA1 levels in PanIN epithelia, acinar cells, and in the fibroinflammatory stroma. Immunohistochemistry is often used in diagnosing various cancers, especially those with

upregulated tumour antigens (Duraiyan *et al*, 2012). Immunohistochemistry staining of HMGA1 is of particular interest because of its various roles in regulating gene expression, embryogenesis, cell differentiation, and adaptive immune responses (Shah *et al*, 2012). By employing IHC staining for HMGA1, we determined that HMGA1 levels are significantly elevated in the nuclei of PanIN epithelial cells, but not in acinar cells or in the fibroinflammatory stroma. This result validates the use of the Ptf1a-Cre; LSL-KrasG12D mouse model for studies investigating how HMGA1 expression levels influence PC progression and for research focussing on HMGA1 as a therapeutic target for treating human cancers in general and PC in particular.

MATERIALS AND METHODS

Animal model and breeding. The scientific name of the LSL Kras G12D mouse strain used was B6.129-Kras tm4Tyj that contains a G12D Kras mutant silenced by a Lox-stop-Lox (LSL) cassette. The scientific name of the P48-Cre mouse strain used was B6.Ptf1a(tm1.1(cre)Cvw) that causes Cre-recombinase expression under control of the Cre knock-in at the Ptf1a-p48 locus that is primarily expressed in the pancreas after embryonic day 9.5. After cross-breeding Kras G12D mice with P48-Cre mice, offspring carrying both genetic elements express Cre-recombinase specifically in the pancreas, thus 'unsilencing' the oncogenic Kras mutant only in the pancreas, leading to PC progression (Hingorani *et al*, 2003). To monitor the progression from precancerous lesions to PC, cohorts of six female mice (double-negative controls and double-positive study) groups at ages 5, 11, and 15 months were generated. Although the IHC study was limited to female mice, standard H&E staining histological analyses of pancreata from male study mice were indistinguishable from female mice, and therefore considered representative of both genders. Mice were bred, sexed, tagged, genotyped, and killed according to procedures approved by the institutional animal care and use committee (IACUC) at Miami University.

Genotyping. Mouse DNA was obtained through an ear punch to determine the genotype of each mouse and to establish individual identities throughout the study. DNA extraction was conducted by submerging the ear punch in 25 μ l of 25 mM NaOH/0.2 mM EDTA at pH 12 and then heating in a thermocycler, GeneAmp PCR System 9700 (Thermo Fisher Scientific, Florence, KY, USA), at 98 °C for 1 h. The samples were then neutralised with 25 μ l of 40 mM Tris-HCl at pH 5. Samples were then stored in -20 °C until PCR amplification was conducted on the DNA with both the Kras and Cre primers. Dreamtaq Green Master Mix (Fisher Scientific, Florence, KY, USA), MgCl₂ (Fisher Scientific), and water were mixed together and either the Kras, Cre, or control primers (IDT, San Jose, CA, USA) were added and then combined with the DNA. For the Kras programme, the mixture was denatured for 30 s at 94 °C, then annealed for 1 min at 69 °C, and elongated for 1 min at 72 °C using the GeneAmp PCR System 9700 (Thermo Fisher Scientific) thermocycler for 35 cycles, then held at 4 °C when complete. For the Cre program, the mixture was denatured for 1 min at 94 °C, then annealed for 20 s at 69 °C, and elongated for 45 s at 72 °C using the thermocycler for 30 cycles, and then held at 4 °C when complete. Gel electrophoresis was then performed using an agarose gel stained with ethidium bromide to separate the amplified gene product. The presence or absence of amplified DNA was determined by inspection under a UV light on the UVP ChemiDoc-It 2 815 Imager (UVP, Upland, CA, USA). If present, the Kras mutation displayed a band at 550 bp and Cre displayed a band at 250 bp. Mice that carried both the Kras mutation and Cre-recombinase were categorised as study mice. Mice that lacked both the Kras mutation and Cre-recombinase were categorised as

control mice. In addition, internal controls were generated from each study mouse by analysing the normal tissue present within the pancreas image. This is further described in the Aperio analysis section.

Pancreata collection, processing, and sectioning. Based on predetermined age ranges, the dates for killing of mice were established. Female mice aged 5, 11, and 15 months were used in this study. These ages were selected based on reports that ~80% of the ducts were normal at 2.25 months, 68% were normal between 4 and 5 months, and 18% were normal between 7 and 10 months in this mouse model (Hingorani *et al*, 2003). Upon killing, pancreatic

tissue samples were collected, stored overnight at room temperature in formalin, and changed to 70% ethanol and placed into 4 °C until further preparation. Pancreatic tissue samples were then processed using the Leica TP 1020 (Leica Biosystems, Buffalo Grove, IL, USA) and embedded using the Shandon Histocentre 3 (Thermo Fisher Scientific). Then, 5 µm sections of each pancreata were made by using Thermo-Shandon Finesse ME Microtome (Thermo Fisher Scientific) and placed on positively charged slides.

IHC staining. Immunohistochemical staining of HMGA1 was conducted at Cincinnati Children's Hospital Medical Center

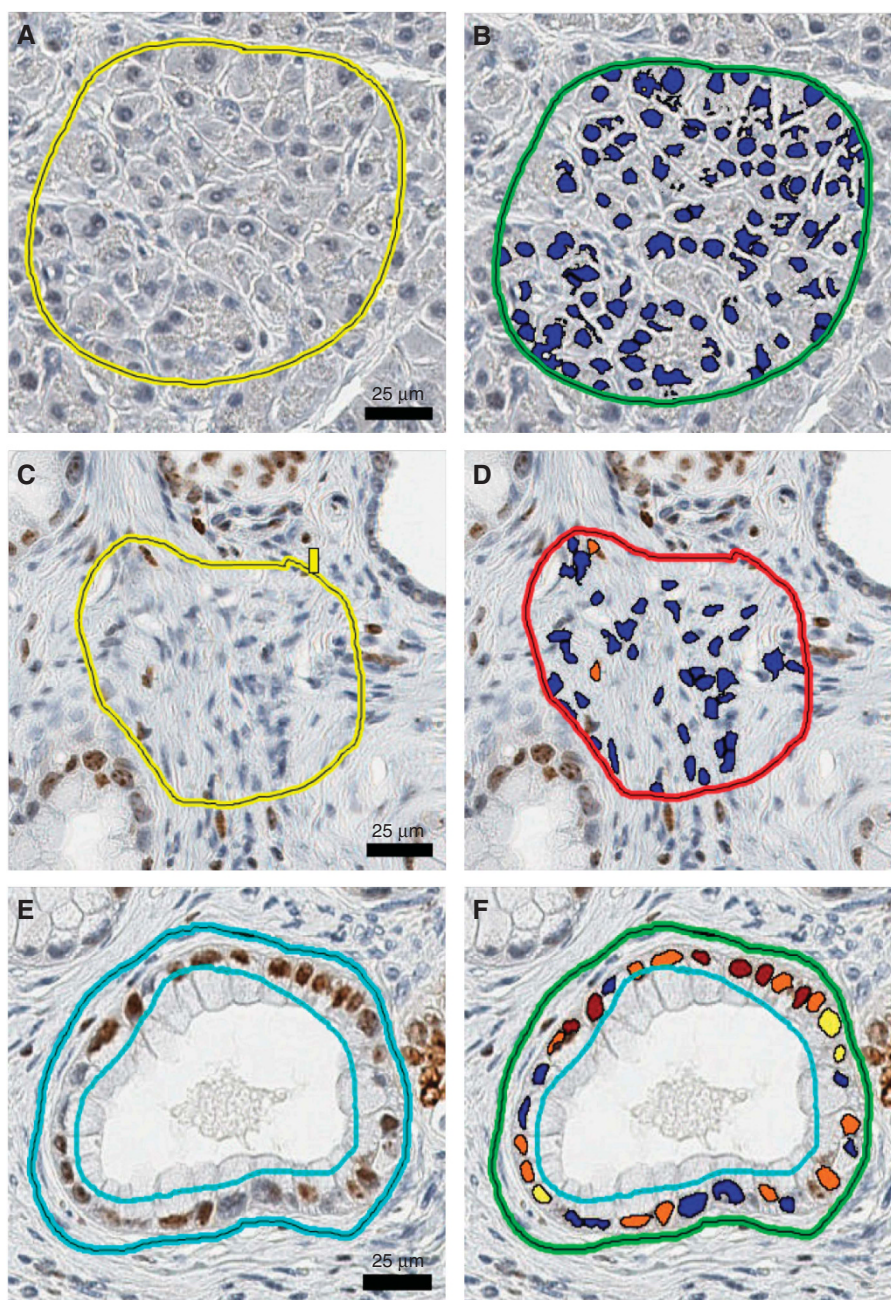


Figure 1. Examples of the nuclear analysis from control and PanIN tissue. (A) Acinar tissue circled as a control for nuclear analysis. (B) Same image as (A) with the nuclear algorithm output. Blue colour represents no staining for HMGA1. (C) Fibroinflammatory stroma circled as control in the 15-month-age category because of lack of acinar tissue. (D) Same image as (C) with the nuclear algorithm output. No staining of HMGA1 is indicated by blue colouring along with two orange-coloured nuclei showing moderate staining. (E) The PanIN circled before the algorithm with an inner circle to exclude nonnuclear PanIN tissue. (F) Same image as (E) with nuclear algorithm workup. The PanIN algorithm displays all staining levels, negative (blue), weak (yellow), moderate (orange), and intense (red). Each image was taken at $\times 20$ in Aperio.

(CCHMC) in the Pathology Research Core. Each slide section was stained with the HMGA1 antibody (ab129153, Abcam, Cambridge, MA, USA) using a fully automated Ventana Discovery XT system (Ventana Medical Systems, Inc., Tuscon, AZ, USA) and following the manufacturer's protocol. The slides were deparaffinised and pretreated in citrate for 32 min. Sections were treated with the HMGA1 antibody in a dilution of 1:2000 for 8 min, followed by treatment with a rabbit secondary antibody (DISCOVERY UltraMap anti-Rb HRP (RUO) 760-4315, Roche, Tucson, AZ, USA) for 12 min. The HRP secondary antibody was used to develop a signal through the use of 3,3'-Diaminobenzidine (DAB) binding to the antigen. The substrate for the HRP was DAB. The Roche OmniMap anti-Rb HRP kit was used and slides were processed using the Discovery XT instrument. Slides were then placed into hematoxylin for 8 min, followed by bluing reagent (Ventana Medical Systems, Inc. (Ventana) Bluing Reagent, 760-2037, Roche) for 4 min. The HMGA1 antibody dilution was 1:2000 from a stock of 100 μ l at 1.631 mg ml⁻¹. Slides were digitally scanned at 20 \times using the Aperio AT2 scanner (Leica Biosystems). Uploaded images were annotated in Aperio eSlide Manager to include regions of interest and the nuclear algorithm was used to conduct the automated analysis of the HMGA1 protein. The specificity of the commercially available HMGA1 antibody has been previously demonstrated (O'Day *et al*, 2015).

Aperio analysis. The HMGA1 is an architectural transcription factor that is localised to the nucleus of cells. Therefore, quantisation of HMGA1 levels was restricted to cellular nuclei. Nuclei quantities and areas were selected by following the instructions in the Aperio IHC Nuclear Image Analysis User's Guide. Internal controls were used to ensure identical IHC staining for control tissue and transformed PanIN tissues. In younger mice that still contained significant amounts of acinar

tissue, 1000 nuclei (± 5 nuclei) were circled from within the acinar tissue to serve as an internal control using Aperio software (Figure 1A and B). In transformed sections of the pancreata, 1000 nuclei (± 5 nuclei) were circled using Aperio software focussing only on PanIN structures (Figure 1E and F). The PanINs, originally thought to be derived from duct cells, were found to be derived from acinar cells with the transformation process being referred to as acinar-to-ductal metaplasia (ADM) (Schmid, 2002; Kopp *et al*, 2012; Prévot *et al*, 2012; Liou *et al*, 2013). In the mouse model used in this study, PanINs and tumours develop from ADM (Hingorani *et al*, 2003). In some of the 15-month images, normal untransformed acinar tissue was absent, or present at amounts that yielded <1000 nuclei (± 5), and therefore fibroinflammatory stroma cells surrounding the PanINs were selected to serve as the internal control nuclei to fulfill the internal control nuclei count (Figure 1C and D). The reactive stroma of the pancreas used as a region to select internal control cells is sometimes referred to as fibroinflammatory stroma that has been described as a transitional tissue that occurs before the display of PanINs (Hruban *et al*, 2001). Although the appearance of reactive stroma or fibroinflammatory stroma is widely present in carcinoma, and pancreatitis, it can also be displayed in normal disease-free pancreatic tissue (Luttges, 1999). After selection of internal control and PanIN nuclei, the nuclear algorithm within the Aperio software was executed and the attributes tables were generated containing the nuclear output layer data (Figure 2). The percent positive nuclei were determined and denoted into four predefined levels in the attributes table (Zarella *et al*, 2016). The levels were represented as follows: none (0) blue, weak (1+) yellow, moderate (2+) orange, and intense (3+) red (See Figure 1F for an example). The standard nuclear algorithm parameters were used in the program. Algorithm parameters, results, and intensity thresholds were examined by pathologist Dr Stringer at CCHMC to ensure correct analysis.

Name	Value
Percent positive nuclei	71.3287
Intensity score	2
(3+) percent nuclei	28.7712
(2+) percent nuclei	24.5754
(1+) percent nuclei	17.982
(0+) percent nuclei	28.6713
Average positive intensity	168.468
Average negative intensity	232.0
(3+) nuclei	288
(2+) nuclei	246
(1+) nuclei	180
(0+) nuclei	287
Total nuclei	1001
Average nuclear RGB intensity	152.37
Average nuclear size (pixels)	127.188
Average nuclear size (μ m ²)	32.0008
Area of analysis (pixels)	704 420
Area of analysis (mm ²)	0.1772

Figure 2. Example of a table of nuclear output data generated by the Aperio software. An example of the nuclear algorithm output generated from an image of a 15-month-old mouse. The percent nuclei, specifically the 3+, 2+, and 1+ values, within this algorithm are used to establish a H Score for each image.

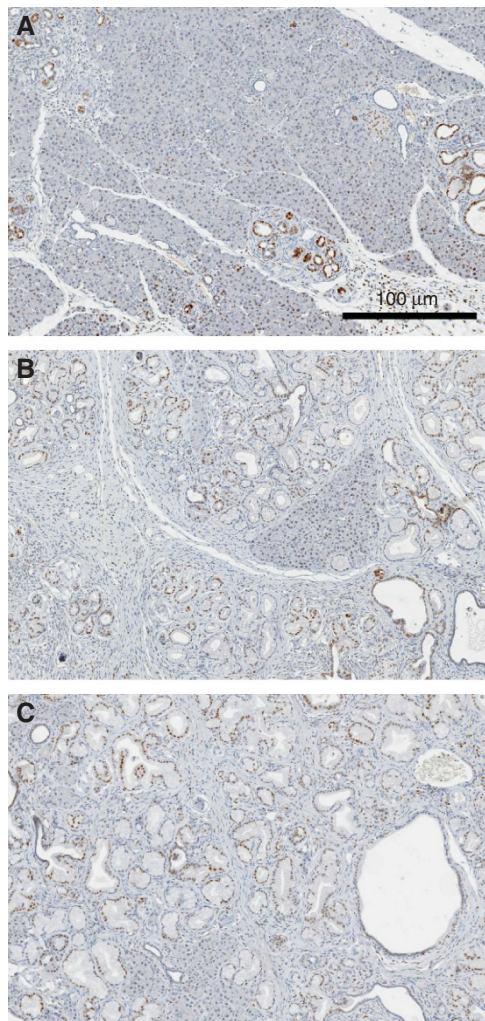


Figure 3. Representative immunohistochemistry-stained sections for each age category. (A) Image from a 5-month-old mouse displaying mostly normal acinar tissue with a few patches of PanINs staining a dark brown colour. (B) Image from an 11-month-old mouse shows mostly PanINs staining dark brown, with a patch of normal acinar cells. (C) Image from a 15-month-old mouse covered with PanINs staining dark brown surrounded by nonstaining cellular stroma. Each image was taken at $\times 5$ in Aperio.

H Score. The H Score was used to quantitatively evaluate HMGA1 level of cellular nuclei after IHC staining. The H Scoring System is similar to the Allred Score System and both are considered to be ‘golden standards’ in IHC analysis, with many investigators establishing alternative IHC analyses based off of these systems (Walker *et al*, 2003; Fedchenko and Reifenrath, 2014; Fitzgibbons *et al*, 2014). The H Score was calculated from the percentage of stained cells and the staining intensity (Detre *et al*, 1995). In the H Scoring System, the H Score is calculated by summing the products of the percent positive cells multiplied by the staining intensities for each group. The staining intensity classification is as follows: 1+ is weak staining, 2+ is moderate staining, and 3+ is strong staining. The equation used to calculate the H Scores was $[(1 \times (\% \text{ cells } 1+)) + (2 \times (\% \text{ cells } 2+)) + (3 \times (\% \text{ cells } 3+))]$. The H Score calculated values ranged from 0 to 300. A score of 300 would mean that all of the cells stained strongly. Based on this scoring system, all control and study IHC images were analysed. The *P*-values, effect sizes, and 95% confidence intervals (CIs) were calculated using the Real Statistics Excel add-in (<http://www.real-statistics.com>).

RESULTS

As expected in the *Ptfla-Cre*; *LSL-KrasG12D* mouse model, the number of PanINs in mouse pancreata increased in the order 5 months, 11 months, and 15 months (Figure 3). Based on visual inspection, mouse pancreata at 5 months of age were mostly composed of normal acinar tissue with scattered pockets of transitioned PanIN tissue (Figure 3A). At 11 months of age, mouse pancreata displayed significantly more PanINs compared with 5-month tissues (Figure 3B). By 15 months of age, most of the acinar tissue in the pancreata had transitioned to PanINs and significant cellular fibroinflammatory stroma was apparent surrounding the PanINs (Figure 3C).

Pancreata IHC stained for HMGA1 from six female mice from each age category were quantified using the Aperio software. Figure 4A–C shows examples of harvested internal control nuclei from untransformed acinar tissue from three different mice from the 5-month-age group. Figure 4D–F shows the resulting scores for each nucleus harvested in the circled region. Nearly all of the internal control nuclei had undetectable levels of HMGA1 indicated by the blue colouring of the processed nuclei. Figure 4G–I shows examples of harvested nuclei from PanINs present in the same three 5-month-old mice. Figure 4J–L shows the same, circled regions processed by the Aperio algorithm, illustrating significant numbers of yellow, orange, and red nuclei, indicating that the PanINs contained weak, moderate, and intense expression levels compared with the negative internal control nuclei. These representative data illustrate the difference in HMGA1 levels observed in nuclei of untransformed acinar cells compared with nuclei of transformed PanIN cells. Supplementary Figure S1A–C shows representative harvested internal control nuclei from untransformed acinar tissue from three different mice from the 11-month-age group. Supplementary Figure S1D–F shows the resulting scores for each nucleus harvested in the circled region. Again, internal control nuclei had mostly undetectable levels of HMGA1 indicated by the blue colouring of the processed nuclei. Supplementary Figure S1G–I shows examples of harvested nuclei from PanINs present in same three 11-month-old mice. Supplementary Figure S1J–L shows the regions processed by the Aperio algorithm, indicating significantly elevated HMGA1 levels in the nuclei of PanIN cells in 11-month-old mice. Finally, in Supplementary Figure S2, 15-month-old mice were typically devoid of untransformed acinar tissue. Therefore, regions of cellular fibroinflammatory stroma were selected as internal controls. Supplementary Figure S2A–C shows examples of harvested internal control nuclei from cells from the stroma from three different mice from the 15-month-age group. Supplementary Figure S2D–F shows the resulting scores for each nucleus harvested by the circled region. Again, nuclei from fibroinflammatory stroma internal control cells had mostly undetectable levels of HMGA1 indicated by the blue colouring of the processed nuclei. Supplementary Figure S2G–I shows harvesting of nuclei from PanINs present in same three 15-month-old mice. Supplementary Figure S2J–L shows the same regions processed by the Aperio software, indicating elevated HMGA1 levels in PanIN epithelia, consistent with that observed in PanIN nuclei in pancreata harvested from 5- and 11-month-old mice.

Figure 5 shows a boxplot analysis of the raw data for the internal controls compared with the PanINs for each age category. The boxplots indicate large separation between the H Scores of internal control nuclei and the H Scores of PanIN nuclei for all age groups compared (Figure 5A). Closer examination of the internal controls for the three groups indicated a slight increase in HMGA1 levels in the nuclei of internal control stroma cells in comparison with nuclei of normal acinar tissue (Figure 5B). Statistical analysis of the H Scores for all comparison between age groups is summarised in

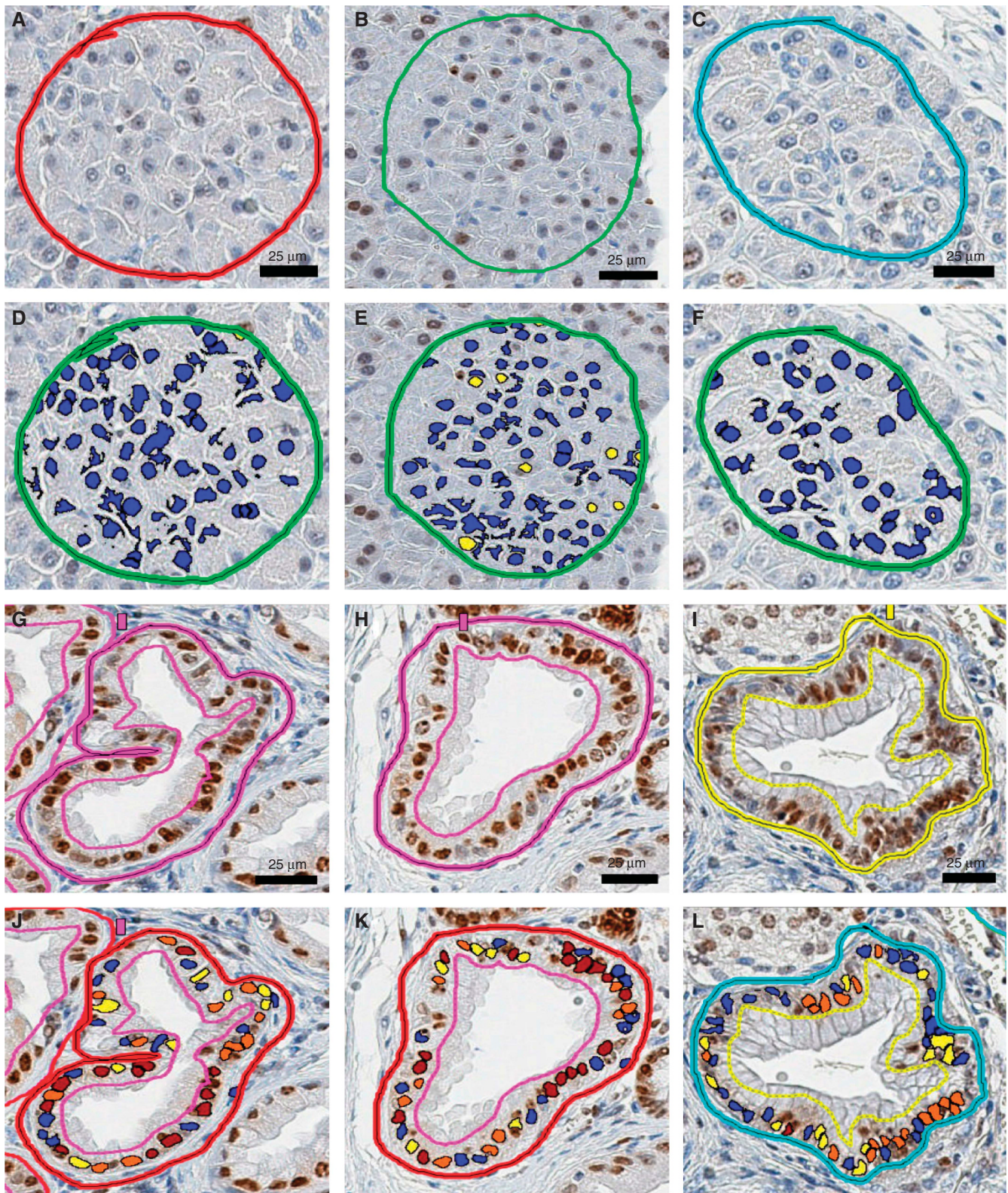


Figure 4. The 5-month nuclear algorithm analysis. (A–C) Examples of internal control acinar tissue circled before running the algorithm. (D–F) The same internal control acinar tissue regions depicted in (A–C), but post nuclear algorithm analysis. (G–I) Example of PanINs circled before the nuclear algorithm analysis. (J–L) The same PanINs as depicted in (G–I), but post the nuclear algorithm analysis. All images were stained for HMGA1 and captured at $\times 20$ in Aperio.

Table 1. Based on the results of a Shapiro–Wilks test for each group, all six groups were found to have normal distributions. Because of the differences in variance between the control and study groups, a one tailed Welch’s *t*-test was conducted between

each age category’s control and study populations. For the 5-month-age group (comparing the control with the study), the *P*-value was found to be 0.00025. The observed effect size was 6.50 between the control and study 5-month-age groups. Based on the

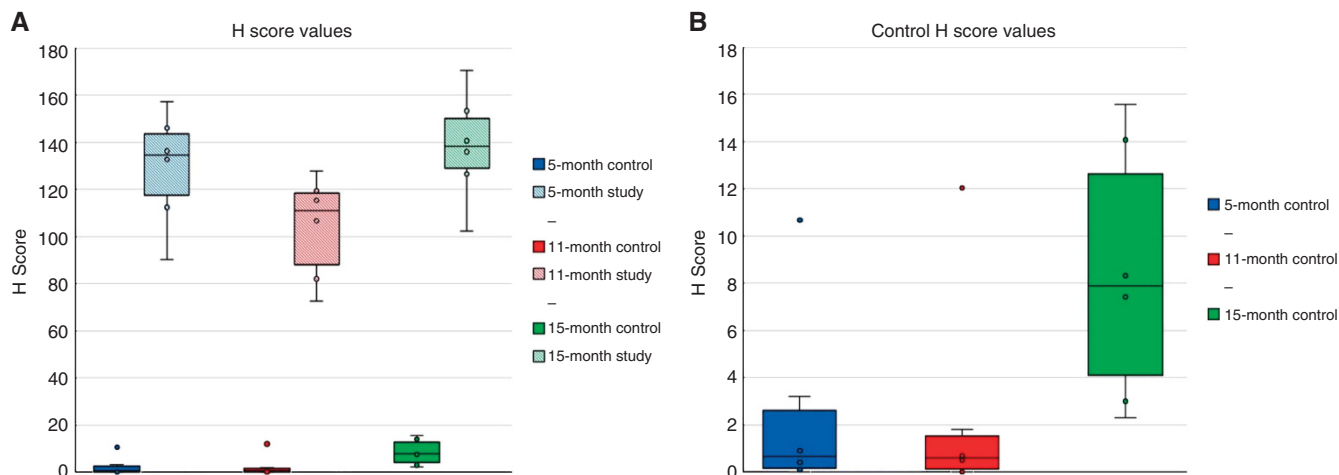


Figure 5. Boxplot graph of H scores from each age category. (A) Boxplot graphs of H Score values from the internal control nuclei and PanIN nuclei for mice aged 5 11, and 15 months. (B) Boxplot graphs of H Score values from the internal controls only to highlight the difference in the measured H Scores between the 5- and 11-month-old mice compared with the 15-month-old mice.

Table 1. H score values and statistical analyses for each age category

Age	Study groups			Internal control groups		
	15	11	5	15	11	5
H-scores	126.57	127.72	136.34	15.57	1.80	0.40
	102.30	106.82	90.19	2.31	0.00	3.20
	170.48	82.06	146.11	14.07	0.00	0.90
	153.45	119.54	112.48	3.00	0.70	0.10
	136.04	72.60	157.16	7.43	0.50	10.68
	140.68	115.53	132.70	7.52	12.04	0.00
Average	138.25	104.04	129.16	8.32	2.51	2.55
St. Dev.	23.28	21.96	24.22	5.50	4.72	4.16
95% CI	18.62	17.57	19.38	3.32	3.77	0.61
Groups compared	15s v. 11s	15s v. 5s	11s v. 5s	15s v. 15ic	11s v. 11ic	5s v. 5ic
P-value	2.57E-02	5.22E-01	8.92E-02	1.55E-04	8.35E-05	2.53E-04
Effect size	1.51	0.38	1.09	7.37	6.36	6.49

Raw H Score values, averages, s.d., and 95% CI are reported for each age category. The P-values and effect sizes for group comparisons are also reported.

P-value and Cohen’s *d* value, it could be concluded that the control group was significantly different and did not belong to the same population as the study group. For the 11-month-age group (comparing the control with the study), the P-value was found to be 0.000084. The observed effect size was 6.36 between the control and study 11-month-age groups. Based on the P-value and Cohen’s *d* value, it could be concluded that the control group was significantly different and does not belong to the same population as the study. Finally, for the 15-month-age group (comparing the internal control population with the study population), the P-value was found to be 0.00016. The observed effect size was 7.37 between the control and study 15-month-age groups. Based on the P-value and Cohen’s *d* value, it could be concluded that the HMGA1 levels in nuclei from the internal control cells of the stroma cells were significantly different compared with that in PanIN cells, and did not belong to the same population of nuclei as the nuclei from the PanIN group of nuclei.

DISCUSSION

The HMGA1 is generally expressed at low levels in normal healthy tissue and HMGA1 expression levels have been shown to be

elevated in cancerous tissue (Fusco and Fedele, 2007; Hristov *et al*, 2010). This study was designed to specifically examine HMGA1 levels in the pancreas over the course of development in the Ptf1aCre; LSL-KrasG12D mouse model for PC. The expression levels of HMGA1 were examined at 5, 11, and 15 months to characterise how HMGA1 expression levels varied in the pancreas tissue at early, intermediate, and late stages of precancerous PanIN development. At 5 months of age, the pancreas was mostly composed of normal acinar tissue with scattered pockets of PanINs. At 11 months of age, mice pancreata displayed a significant increase in transformed PanINs compared with pancreatic tissue at 5 months of age, with PanINs typically comprising more than half of the pancreas tissue accompanied by an increasing amount of fibroinflammatory stroma. By the age of 15 months, pancreata were typically entirely composed of PanINs surrounded by a significant amount of fibroinflammatory stroma. It should be noted that the progression from normal healthy pancreas, dominated by exocrine acinar tissue, to a tissue essentially composed entirely of PanINs and fibroinflammatory stroma, proceeds initially by the transformation of acinar tissue to PanINs in a process referred to as ADM, where metaplasia refers to the transformation or replacement of one cell type by another, that is, transformation or replacement of acinar cells by PanIN epithelial cells. As the mouse ages, there is increased progression

from localised replacement of acinar cells by PanINs to a more disorganised tissue structure characterised by wholesale conversion of acinar tissue to PanINs with significant emergence of fibroinflammatory stroma that precedes cancer initiation.

Our results indicated that HMGA1 levels were essentially below detection in normal acinar tissue and in the complex reactive cellular stroma surrounding PanINs, but significantly elevated in nuclei of established PanINs. The pancreatic adenocarcinoma stroma is known to be composed of both cellular and acellular components, including fibroblasts, myofibroblasts, pancreatic stellate cells, immune cells, blood vessels, extracellular matrix, cytokines, and growth factors (Waghray *et al*, 2013). Once acinar cells transformed into PanIN epithelial cells, we could not detect any further increase in the HMGA1 levels in PanIN cellular nuclei with increasing age. From our data, we cannot make any conclusion regarding whether or not elevated HMGA1 expression levels in acinar cells precede ADM and PanIN formation, but our data clearly show that HMGA1 expression levels are a hallmark and a characteristic of PanIN epithelial cells once they have been established by the process of ADM. Although HMGA1 expression levels are generally not elevated in the fibroinflammatory stroma surrounding established PanINs, a significant increase in HMGA1 content was observed in the stroma in the 15-month-old mice in comparison with the 5- and 11-month-old mice, reflecting HMGA1 expression in an increasing population of PC stellate cells in the stroma as the pancreas tissue approaches a transition to adenocarcinoma.

Although the precise role that HMGA1 plays in PC progression and the precise mechanism that elevated HMGA1 levels play in acinar to ductal metaplasia remains unknown, it is well established that HMGA1 expression levels are elevated in the cells of many human cancers. Therefore, elevated HMGA1 expression levels are considered a hallmark of many human cancers. Consequently, HMGA1 is receiving growing attention as a cancer biomarker and as a potential target for cancer therapy and treatment. Given the growing appreciation of the importance of HMGA1 in cancer progression, and the heavy reliance on mouse models for PC research, the results presented here validate the use of the Ptf1aCre; LSL-KrasG12D mouse model for studies investigating the role that HMGA1 plays in cancer progression, and for research targeting HMGA1 as a potential anticancer therapeutic target (Liau and Whang, 2008; Shah and Resar, 2012).

ACKNOWLEDGEMENTS

We thank pathologist Dr Keith Stringer at Cincinnati Children's Hospital Medical Center for his assistance with the examination of the nuclear algorithms. This work was supported by a grant from the NIH/NCI (1R15CA152985) awarded to MAK.

CONFLICT OF INTEREST

The authors declare no conflict of interest.

REFERENCES

- American Cancer Society (2017) *Cancer Facts & Figures 2017*. American Cancer Society: Atlanta, GA, USA.
- Chari ST, Kelly K, Hollingsworth MA, Thayer SP, Ahlquist DA, Andersen DK, Batra SK, Brentnall TA, Canto M, Cleeter DF, Firpo MA, Gambhir SS, Go VL, Hines OJ, Kenner BJ, Klimstra DS, Lerch MM, Levy MJ, Maitra A, Mulvihill SJ, Petersen GM, Rhim AD, Simeone DM, Srivastava S, Tanaka M, Vinik AI, Wong D (2015) Early detection of sporadic pancreatic cancer: summative review. *Pancreas* **44**(5): 693–712.
- Detre S, Saclani JG, Dowsett M (1995) A 'quickscore' method for immunohistochemical semiquantitation: validation for oestrogen receptor in breast carcinomas. *J Clin Pathol* **48**(9): 876–878.
- Duraiyan J, Govindarajan R, Kaliyappan K, Palanisamy M (2012) Applications of immunohistochemistry. *J Pharm Bioallied Sci* **4**: S307–S309.
- Fedchenko N., Reifenrath J (2014) Different approaches for interpretation and reporting of immunohistochemistry analysis results in the bone tissue—a review. *Diagn Pathol* **9**: 221.
- Fesinmeyer MD, Austin MA, Li CI, De Roos AJ, Bowen DJ (2005) Differences in survival by histologic type of pancreatic cancer. *Cancer Epidemiol Biomarkers Prev* **14**(7): 1766–1773.
- Fitzgibbons PL, Dillon DA, Alsabeh R, Berman MA, Hayes DF, Hicks DG, Hughes KS, Nofech-Mozes S (2014) Template for reporting results of biomarker testing of specimens from patients with carcinoma of the breast. *Arch Pathol Lab Med* **138**(5): 595–601.
- Fusco A, Fedele M (2007) Roles of HMGA proteins in cancer. *Nat Rev Cancer* **7**: 899–910.
- Futura K, Watanabe H, Ikeda S (1992) Differences between solid and duct-ectatic types of pancreatic ductal carcinomas. *Cancer* **69**(6): 1327–1333.
- Hingorani SR, Petricoin EF, Maitra A, Rajapakse V, King C, Jacobetz MA, Ross S, Conrads TP, Veenstra TD, Hitt BA, Kawaguchi Y, Johann D, Liotta LA, Crawford HC, Punt ME, Jacks T, Wright CV, Hruban RH, Lott AM, Tuveson DA (2003) Preinvasive and invasive ductal pancreatic cancer and its early detection in the mouse. *Cancer Cell* **4**(6): 437–450.
- Hristov AC, Cope L, Cello FD, Reyes MD, Singh M, Hillion J, Belton A, Joseph B, Schuldenfrei A, Iacobuzio-Donahue C, Maitra A, Resar LMS (2010) HMGA1 correlates with advanced tumor grade and decreased survival in pancreatic ductal adenocarcinoma. *Mod Pathol* **23**(1): 98–104.
- Hruban RH, Adsay NV, Albores-Saavedra J, Compton C, Garrett ES, Goodman SN, Kern SE, Klimstra DS, Kloppel G, Longnecker DS, Luttges J, Offerhaus GJ (2001) Pancreatic intraepithelial neoplasia (PanIN): a new nomenclature and classification system for pancreatic duct lesions. *Am J Surg Pathol* **25**(5): 579–586.
- Jackson EL, Willis N, Mercer K, Bronson RT, Crowley D, Montoya R, Jacks T, Tuveson DA. (2001) Analysis of lung tumor initiation and progression using conditional expression of K-ras. *Genes Dev* **15**: 3243–3248.
- Jemal A, Siegel R, Ward E, Murray T, Xu J, Smigal C, Thun MJ (2006) Cancer statistics. *CA Cancer J Clin*. **56**(2): 106–130.
- Johnson L, Mercer K, Greenbaum D, Bronson RT, Crowley D, Tuveson DA, Jacks T (2001) Somatic activation of the K-ras oncogene causes early onset lung cancer in mice. *Nature* **410**: 1111–1116.
- Kawaguchi Y, Cooper B, Gannon M, Ray M, MacDonald RJ, Wright CV (2002) The role of the transcriptional regulator Ptf1a in converting intestinal to pancreatic progenitors. *Nat Genet* **32**(1): 128–134.
- Kolb S, Fritsch R, Saur D, Reichert M, Schmid RM, Schneider G (2007) HMGA1 controls transcription of insulin receptor to regulate cyclin D1 translation in pancreatic cancer cells. *Cancer Res* **67**(10): 4679–4686.
- Kopp JL, Figura G, Mayes E, Liu F, Dubois CL, Morris JP, Pan FC, Akiyama H, Wright CVE, Jensen K, Hebrok M, Sander M (2012) Identification of Sox9-dependent acinar-to-ductal reprogramming as the principal mechanism for initiation of pancreatic ductal adenocarcinoma. *Cancer Cell* **22**(6): 737–750.
- Liau SS, Whang E (2008) HMGA1 is a molecular determinant of chemoresistance to gemcitabine in pancreatic adenocarcinoma. *Clin Cancer Res* **14**(5): 1470–1477.
- Liau SS, Whang E (2009) High mobility group A: a novel biomarker and therapeutic target in pancreatic adenocarcinoma. *Surgeon* **7**: 297–306.
- Liou GY, Döppler H, Necela B, Krishna M, Crawford HC, Raimondo M, Storz P (2013) Macrophage-secreted cytokines drive pancreatic acinar-to-ductal metaplasia through NF- κ B and MMPs. *J Cell Biol* **202**(3): 563–577.
- Luttges J (1999) Metaplasia in the pancreas. *Rev Esp Pathol* **23**(3): 441–442.
- National Cancer Institute (2014) *Scientific Framework for Pancreatic Ductal Adenocarcinoma (PDAC)*. National Institutes of Health: Bethesda, MD, USA.
- Ottendorf NA, Milne AN, Morsink FH, Drillenburger P, Ten Kate FJ, Maitra A, Offerhaus GJ (2009) Pancreatic intraepithelial neoplasia and pancreatic tumorigenesis: of mice and men. *Arch Pathol Lab Med* **133**(3): 375–381.
- O'Day E, Le MTN, Imai S, Tan SM, Kirchner R, Arthanari H, Hofmann O, Wagner G, Lieberman J (2015) An RNA-binding protein, Lin28, recognizes and remodels G-quartets in the microRNAs (miRNAs) and mRNAs it regulates. *J Biol Chem* **290**(29): 17909–17922.

- Prévoit PP, Simion A, Grimont A, Colletti M, Khalaileh A, Van den Steen C, Xu X, Roelants V, Hald J, Bertrand L, Heimberg H, Konieczny SF, Dor Y, Lemaigre FP, Jacquemin P (2012) Role of the ductal transcription factors HNF6 and Sox9 in pancreatic acinar-to-ductal metaplasia. *Gut* **61**(12): 1723–1732.
- Puca F, Colamaio M, Federico A, Gemei M, Tosti N, Uchimura Bastos A, Del Vecchio L, Pece S, Battista S, Fusco A (2014) HMGA1 silencing restores normal stem cell characteristics in colon cancer stem cells by increasing p53 levels. *Oncotarget* **5**(10): 3234–3245.
- Rahib L, Smith BD, Aizenberg R, Rosenzweig AB, Fleshman JM, Matrisian LM (2014) Projecting cancer incidence and deaths to 2030: the unexpected burden of thyroid, liver, and pancreas cancers in the United States. *Cancer Res* **74**(11): 2913–2921.
- Schmid RM (2002) Acinar-to-ductal metaplasia in pancreatic cancer development. *J Clin Invest* **109**(11): 1403–1404.
- Shah SN, Kerr C, Cope L, Zambidis E, Liu C, Hillion J, Belton A, Huso DL, Resar LMS (2012) HMGA1 reprograms somatic cells into pluripotent stem cells by inducing stem cell transcriptional networks. *PLoS One* **7**(11): e48533.
- Shah SN, Resar LM (2012) High mobility group A1 and cancer: potential biomarker and therapeutic target. *Histol Histopathol* **27**(5): 567–579.
- Siegel RL, Miller KD, Jemal A (2016) Cancer statistics, 2016. *CA Cancer J Clin* **66**(1): 7–30.
- Stark A, Eibl G (2015) Pancreatic ductal adenocarcinoma. *Pancreapedia: Exocrine Pancreas Knowledge Base*. Version 1.0, pages 1–9. University of Michigan: Ann Arbor, MI, USA.
- Tuveson DA, Shaw AT, Willis NA, Silver DP, Jackson EL, Chang S, Mercer KL, Grocjow R, Hock H, Crowley D, Hingorani SR, Zaks T, King C, Jacobetz MA, Wang L, Bronson RT, Orkin SH, DePinho RA, Jacks T (2004) Endogenous oncogenic K-rasG12D stimulates proliferation and widespread neoplastic and developmental defects. *Cancer Cell* **5**(4): 375–387.
- Waghray M, Yalamanchili M, di Magliano MP, Simeone DM (2013) Deciphering the role of stroma in pancreatic cancer. *Curr Opin Gastroenterol* **29**(5): 537–543.
- Walker RA, Harris AL, Balslev E (2003) Immunohistochemistry and breast cancer diagnosis, therapy and prognosis. *Danish Pathology Society (DPAS)* **2003**: 1–10.
- Warshaw AL, del Castillo FC (1992) Pancreatic carcinoma. *N Engl J Med* **326**(7): 455–465.
- Watanabe M, Sheriff S, Lewis KB, Tinch SL, Cho J, Balasubramaniam A, Kennedy MA (2012) HMGA-targeted phosphorothioate DNA aptamers increase sensitivity to gemcitabine chemotherapy in human pancreatic cancer cell lines. *Cancer Lett* **315**: 18–27.
- Yadav D, Lowenfels AB (2013) The epidemiology of pancreatitis and pancreatic cancer. *Gastroenterology* **144**(6): 1252–1261.
- Zarella E, Coulter M, Welsh A, Carvajal D, Schalper K, Harigopal M, Rimm D, Neumeister V (2016) Automated measurement of estrogen receptor in breast cancer: a comparison of fluorescent and chromogenic methods of measurement. *Lab Invest* **96**(9): 1016–1025.

This work is published under the standard license to publish agreement. After 12 months the work will become freely available and the license terms will switch to a Creative Commons Attribution-NonCommercial-Share Alike 4.0 Unported License.

Supplementary Information accompanies this paper on British Journal of Cancer website (<http://www.nature.com/bjc>)